Climatic Change (2025) 178:95
https://doi.org/10.1007/s10584-025-03940-5

Detection and attribution of trends of meteorological extremes in Central America

H. G. Hidalgo[1] · S. W. Chou-Chen[2] · K. A. McKinnon[3] · S. Pascale[4] · D. Quesada-Chacón[5] · E. J. Alfaro[6] · P. Bautista-Solís[7] · P. M. Pérez-Briceño[8] · H. F. Diaz[9] · T. Maldonado[10] · E. R. Rivera[11] · T. Nakaegawa[12]

Received: 5 September 2024 / Accepted: 19 April 2025

Abstract
We present an analysis to determine whether historical trends in extreme precipitation and temperature indices, as well as in yearly averages of several climate variables. To achieve this, we use three methodologies: a) a climate model-based approach, b) a hybrid method that combines models and observations (1979–2019), and c) a climate observations-based method (1983–2016). For each methodology, we compare the climate change *signal*, represented by the historical trends, to the *noise* generated by simulated climate datasets (using models or statistical methods) that do not include human influence. Overall, the model-based method suggests possible detection of the human influence in most temperature extreme indices and in precipitation-related indices in the northern countries. The hybrid method detects human influence in significantly fewer variables, but in many cases, consistently with those of the model-based approach. Both the hybrid and observation-based methods exhibit similar noise variability to the model-based method. Notably, due to limitations in data availability, our analysis excludes the most recent five years, during which substantial warming and an increase of extreme events have been observed globally.

Keywords Extreme events · Detection and attribution · Anthropogenic climate change · Central America

1 Introduction

Central America has emerged as the most prominent hot-spot for climate change in the tropics, primarily due to a substantial reduction in projected precipitation and an increase in precipitation variability in response to global warming (Giorgi 2006; Donatti et al. 2024). The intensification of the water cycle in a warmer climate (Trenberth et al. 2003; Held and Soden 2006), coupled with the overall rise in global mean temperatures, is expected to exacerbate extreme weather events in this region, including precipitation, droughts and temperature extremes (Arias et al. 2021; Seneviratne et al. 2021). Located near the center of action of El Niño-Southern Oscillation (ENSO) and influenced by various remote sea surface tempera-

Extended author information available on the last page of the article

Published online: 30 April 2025

ture (SST) drivers from nearby ocean basins (see the summary table of climate precursors in Ley et al. 2023), climate extremes are heavily influenced by natural climate variability in the Central American isthmus. Along with the large effects of internal climate variability, the complex topography of Central America also results in a myriad of microclimates, making it particularly challenging to disentangle natural versus anthropogenic signals on climatic extremes (e.g., Neelin et al. 2006; Pascale et al. 2021; Anderson et al. 2023).

Droughts are common in the Central America Dry Corridor (CADC; Gotlieb et al. 2019; Hidalgo et al. 2019; Morataya-Montenegro and Bautista-Solís 2020; Ley et al. 2023), a region characterized by relatively high aridity that extends from southern Mexico to El Salvador, including the Pacific coast of Nicaragua and the Guanacaste province in Costa Rica. Some authors also consider the "Dry Arc" ("Arco Seco" in Spanish) region in Panama to be a discontinuous part of this corridor. The climate variability of the CADC is heavily influenced by ENSO, variability of SSTs in the Caribbean and tropical North Atlantic, the Caribbean Low Level Jet (CLLJ; Amador 1998, 2008), which is a consistent wind pattern of strong zonal winds in the Caribbean basin at around 925 hPa with velocities that can reach around 10 m s^{-1}, as well as other remote drivers such as the Pacific Decadal Oscillation (PDO; Mantua et al. 1997) and the Atlantic Multidecadal Oscillation (Enfield et al. 2001). In addition, another important control on precipitation in Central America is the interbasin (tropical Pacific minus tropical Atlantic) sea surface temperature (SST) difference (e.g. Enfield and Alfaro 1999; Fuentes-Franco et al. 2015; Alfaro et al. 2016; Maldonado et al. 2017; Hidalgo et al. 2017; Romero and Alfaro 2024). Droughts severely impact the CADC, a region whose inhabitants largely rely on rainfed agriculture (Gotlieb et al. 2019; Hidalgo et al. 2019; Ley et al. 2023; Cavazos et al. 2024). This dependence creates critical social and economic vulnerabilities.

In contrast, floods occur over shorter time scales but can have devastating effects. Various mechanisms, of both tropical and extratropical origin—convective storms, cold fronts, synoptic scale gyres, easterly waves, tropical cyclones– can deliver massive amounts of rainfall just in a few days, causing landslides, flooding, and significant impacts on human systems (Pérez-Briceño et al. 2016; Guevara-Murua et al. 2018; González-Trujillo et al. 2024).

Finally, temperature extremes—measured by, e.g., the heat index– have been on the rise in Central America in the last few decades. This increase is driven by changes that lead to more anomalous high-pressure systems, enhancing sinking air, and warm/weaker cold advection (Angeles-Malaspina et al. 2018). The frequency of extreme temperature events has also intensified since 1991, with the highest occurrences during the cool phase of ENSO (Ramirez-Beltran et al. 2017). Record breaking heat was observed in Central America as recenty as 2023 (Perkins-Kirkpatrick et al. 2024). Heat waves in Central America are associated with adverse impacts on human health (Miranda-Chacón et al. 2023; Baker 2023) and in biodiversity (González-Trujillo et al. 2024).

Given the significant socio-economic impacts of meteorological and climatic extremes on Central America, where there is a high vulnerability and exposure to natural hazards, it is important to determine if these trends in extreme events observed in recent decades can be attributed to anthropogenic climate change, as this may indicate that human activities are already influencing these observed changes, as seen in other regions (Kawase et al. 2023), and therefore, we can expect that these extremes to continue worsening and not to reverse in the future as part of a multidecadal cycle.

This article presents a study on the detection and attribution of extreme climatic event, focusing on indices such as annual precipitation, annual temperature, annual potential evapotranspiration, aridity index and seasonal precipitation. The objective of this type of studies is to determine whether the anthropogenic signal, in a historical climate, emerges over the amplitude of the internal natural variability noise (which can be assessed through control simulations or statistical models). Three methods were employed in this study: a) a *model-based framework*, using signals derived from historical climate runs and noise extracted from preindustrial control runs (piCONTROL). These runs come from a suite of 10 models from the Coupled Model Intercomparison Project Phase 6 (CMIP6) downscaled and processed by the Inter-Sectoral Impact Model Intercomparison Project's round 3 (ISIMIP3, https://data.isimip.org/); b) a *model-observations hybrid method,* in which the trend signal is taken from dynamically downscaled reanalysis data while the noise is constructed from a synthetic (statistical) ensemble based on observed main large-scale climate precursors, and c) an *observation-based framework*, in which the signal is derived from observed trends, and the noise is calculated in the same manner as in the previous hybrid method. This study aims to compare these methods and identify which climate variables have already shown evidence of human impact.

In Central America, particularly in the CADC subregion, there is a substantial body of observational studies focusing on trends in precipitation (Aguilar et al. 2005; Neelin et al. 2006; Hidalgo et al. 2017; Pascale et al. 2019; Alfaro-Córdoba et al. 2020, 2024). However, there are relatively fewer studies addressing detection and attribution of these trends (Pascale et al. 2021; Anderson et al. 2023) or exploring climate extremes (Aguilar et al. 2005; Alfaro-Córdoba et al. 2024). Our study represents an important advancement in this field, as it examines both issues and estimates the detection and attribution of climate trends related to more extreme phenomena (precipitation, droughts, temperature) using multiple observation sources. Previous research on detection and attribution in the region includes studies by Pascale et al. (2021) and Anderson et al. (2023). These studies investigated multidecadal precipitation trends from 1979 to 2019 and the 2015–2019 multi-year drought in Central America (see also studies of trends in Central America in Neelin et al. 2006 and Hidalgo et al. 2017). Specifically, Pascale et al. (2021) found that the precipitation trend was not beyond what could be expected by natural variability alone, while the 2015–2019 drought was exacerbated by anthropogenic forcing. Anderson et al. (2023) reported that the drought was rare within the range of natural variability, but it might still be linked to natural causes. Clearly, there is a gap in the literature regarding comprehensive attribution studies of temperature and precipitation extremes in Central America, which our study tries to identify and address.

2 Data

2.1 Model and hybrid data

Several climate datasets were obtained from ISIMIP3 to compute the natural variability noise and the models' historical trends, with the aim to detect and attribute these trends to anthropogenic anthropogenic sources. The W5E5 v2.0 dataset (Lange et al. 2021) was employed as hybrid data. W5E5 merges WFDE5 (Weedon et al. 2014; Cucchi et al. 2020),

a bias-adjusted version of ERA5 (Hersbach et al. 2020) over land, with raw ERA5 data over the ocean. It provides global coverage at 0.5° resolution with daily data from 1979 to 2019. Even though the W5E5 dataset has not been validated for Central America, the original data from the ERA5 reanalysis have shown significant skill in reproducing precipitation in the region (Stewart et al. 2021).

Additionally, as model data, we used both the preindustrial control (piCONTROL, 500 years of simulation) and the historical (from 1850 to 2014) runs concatenated with the SSP5 - 8.5 scenario, to extend it to 2016 for ten CMIP6 General Circulation Models (GCMs; see Table S1 of the Supplementary Information).. These datasets were downscaled and bias-adjusted to W5E5 with ISIMIP3's bias adjustment and statistical downscaling algorithm (ISIMIP3BASD; Lange 2019, 2022), and are available at Lange and Büchner (2021), Lange et al. (2023a) and Lange et al. (2023b). The selected downscaled variables for the ISIMIP3 datasets include daily precipitation (P), surface maximum temperature (Tx) and minimum temperature (Tn), all at 0.5° × 0.5° horizontal resolution.

2.2 Observed and blended (observations and satellite data)

A blend of satellite and meteorological station precipitation data of the Climate Hazards and Infrared Precipitation with stations (CHIRPs; Funk et al. 2015) was used to represent "observations" from 1981 to 2020. This data is at a 5 km horizontal resolution but has been aggregated to a 0.5° × 0.5° grid to align with the models. Similarly, Tx and Tn data were obtained from a corresponding dataset for temperature (CHIRTs; Funk et al. 2019) for the period 1983 − 2016. Both CHIRPs and CHIRTs datasets have shown good agreement with station data in several locations of Central America and the Caribbean region (Anderson et al. 2019; Quesada-Hernández et al. 2019; Centella-Artola et al. 2020; Stewart et al. 2021; Ugalde 2022; Alfaro-Córdoba et al. 2024). These data were used to calculate observed trends in precipitation and temperature indices for the historical period of interest for 5 subregions in Central America. A common period from 1983 to 2016 was chosen for both datasets. The data were converted to the ISIMIP3 grid at 0.5 × 0.5 degrees horizontal resolution using the "nearest" method.

2.3 Observed atmospheric and oceanic climate indices that relate to Central America's terrestrial climate

Monthly indices for main modes of climate variability that affect Central America (Maldonado et al. 2018; Durán-Quesada et al. 2020; Anderson et al. 2023) were obtained from the National Oceanic and Atmospheric Administration (NOAA) Physical Sciences Laboratory (https://psl.noaa.gov/gcos_wgsp/Timeseries/, last visit 4/8/2024). These data were used to generate the natural variability noise for the detection and attribution analysis through a synthetic method (McKinnon and Deser 2021; Anderson et al. 2023). The indices obtained were the *Niño3.4* index for ENSO, defined as the SST anomaly over the region 5°N–5°S, 170–120°W, and the Pacific Decadal Oscillation (*PDO*; Mantua et al. 1997), defined as the time history of the leading EOF of North Pacific SST. We also used an index for the Caribbean Low-level Jet (*CLLJ*; Amador 1998, 2008, Amador et al. 2018; Hidalgo et al. 2015; 2019; Anderson et al. 2023), defined as area-average of the 925 hPa zonal wind over the domain 12.5–17.5°N and 80–70°W (Wang 2007). Following Amador et al. (2018), in order

to generate a *CLLJ* time series that matches the length of the other indices, the 1900–2022 time series was constructed by combining data from two sources: the NOAA-CIRES-DOE 20 th Century Reanalysis (20 CRv3) *CLLJ* index from 1920 to 1948 and the International Research Institute (IRI) at Columbia University *CLLJ* Index from 1949 to 2019, which is based on National Center for Environmental Prediction/National Center of Atmospheric Research (NCEP-NCAR) Reanalysis data (Kalnay et al. 1996). We performed a homogenization procedure by imposing the mean and standard deviation of the 1951–2006 period of the IRI data to the entire length of the concatenated time series. This period chosen to align with the original baseline period of the NOAA NCEP-NCAR CDAS- 1 zonal wind dataset used to calculate the IRI index. Finally, to account for anthropogenic effects, we selected the smoothed Global Mean Temperature (GMT), following the methodology used in previous studies (Hawkins et al. 2020; Hyun et al. 2020; Ying et al. 2022; Anderson et al. 2023). Anderson et al. (2023) justify the use of GMT over a regional temperature average to represent the forced component, as GMT is less likely to contain unforced local "noise". This ``noise'' is captured by othe natural variability terms such as the climate variability modes mentioned before. However, instead of using climate model data for this component, as done by Anderson et al. (2023), we based our analysis on observed data from surface or satellite sources, without incorporating any climate model data. In our case, we used the GISS Surface Temperature Analysis (GISTEMP v4; GISTEMP Team 2024; Lenssen et al. 2019) dataset for this representation. As in McKinnon and Deser (2021) and Anderson et al. (2023), the anthropogenic forcing (*Ft)* was smoothed using a 1/10-year low-pass filtered version of the SST time series. Additionally, the *PDO* was orthogonalized with respect to ENSO, due to their relatively strong intercorrelation, and it is referred to as PDO_{perp} hereinafter.

3 Methods

3.1 Calculation of climatological and extreme indices

Model and observed daily data were used to calculate the following indices:

(a) *Extreme event indices*: A total of 10 precipitation indices (Table S2 of the Supplementary Information) to characterize extreme events were calculated for each grid point defining the clusters shown in Fig. 1, as described in Aguilar et al. (2005). These indices are also part of the CLIMDEX project (https://www.climdex.org) and are included in Climpact (https://github.com/ARCCSS-extremes/climpact/blob/master/www/user_guide/Climpact_user_guide.md#appendixa) indices, which will be merged into CLIMDEX (Nakaegawa and Murazaki 2022). Similarly, 11 extreme temperature indices (Table S3 of the Supplementary Information) were computed using Tx and Tn data.

(b) *Annual indices*: We used annual averages of P, temperature (T), potential evapotranspiration (PET)—calculated using Thornthwaite (1948)—and the aridity index (ϕ), defined as the yearly ratio of water supply (P) to water demand (PET) as:

$$\phi = \frac{P}{PET} \tag{1}$$

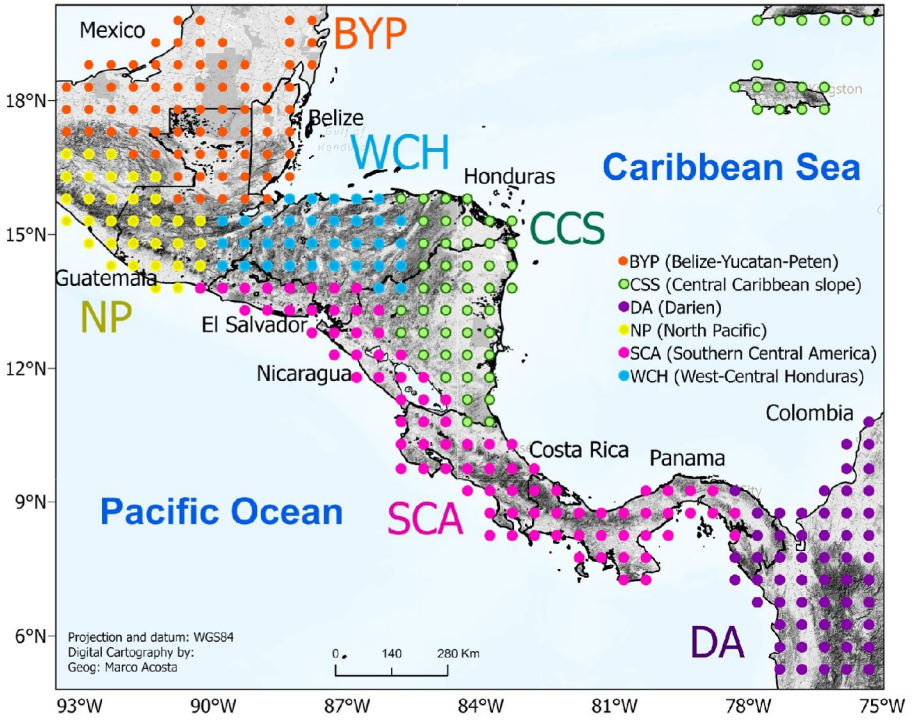

Fig. 1 Hierarchical clusters using data derived from the CLIMDEX extreme indices for precipitation and temperature (tables S2 and S3 of the Supplementary Information), and annual averages of precipitation (P), 2-m temperature (T), potential evaporation (PET) and the ϕ aridity index (defined as P/PET). The cluster for Darien (DA) was not analyzed in following sections due to its small area that has limited meteorological observations because of its inaccessibility. The data covers the period from 1983 to 2016. The identified clusters are: Belize-Yucatan-Peten (BYP), West-Central Honduras (WCH), Southern Central America (SCA), Central Caribbean slope (CCS), North Pacific (NP) and Darien (DA)

Therefore, a smaller ϕ is associated with higher aridity.

(c) *Seasonal indices*: We also studied seasonal precipitation during the boreal seasons: December-January–February precipitation (PDJF), March–April-May precipitation (PMAM), June-July–August precipitation (PJJA) and September–October-November precipitation (PSON). While a large part of the Pacific slope is characterized by a well-defined dry season and Mid-Summer Drought (Magaña et al. 1999; Garcia-Franco et al. 2022), other type of "tropical seasons" may be more suitable. However, we chose not to use them because they do not align with the climatology of subregions in the Caribbean slope.

A total of 29 variables (10 extreme precipitation indices, 11 extreme temperature indices, 4 annual series and 4 seasonal series) for the historical period were prepared for the analysis limited by the period of observations (1983–2016), but for the hybrid method the period of 1979–2019 was used. Regarding the "noise" representing natural climate variability, the same 29 variables were calculated, but the periods varied according to the two methods for computing climate variability noise, which will be explained later. The possible 34-years

trends for the 29 variables of all standardized simulations and observations were computed in all models runs and synthetic simulations.

3.2 Cluster analysis

A hierarchical cluster analysis (Wilks 2019) was performed using a set of all standardized time series for the extreme variables from the CHIRPs and CHIRTs data, alongside annual P, T, PET and ϕ over the 1983–2016 period. Several cutoff levels were tested until the data was successfully divided in 5 regular size clusters: Belize-Yucatan-Peten (BYP), West-Central Honduras (WCH), Southern Central America (SCA), Central Caribbean slope (CCS), North Pacific (NP) and a smaller one that represented a small area in the Darien subregion (DA; Fig. 1). However, because the Central American portion of this latter cluster is very small and located in a region with low observational confidence due to the absence of meteorological stations in the inhospitable Darien jungle, no analysis is presented on that cluster.

The signal trend is calculated from the standardized versions of the variables using linear regression, and it is represented by the dots in Fig. 2. The noise (shown as bars) is determined by the distances between the mean (which is approximately zero in all cases) of the trend distribution and the 97.5—2.5 percentiles of the same distribution. These bars are centered on each dot to account for two-tail bounds as the sign of the trend is not known a-priori. This is why the bars are centered over the dots. If the bars do not cross the zero line, it indicates a detectable trend in that variable, and vice versa. This is equivalent to plotting the confidence intervals of the noise trend distribution, which are centered on the x-axis and the signal; with the signal being closer to one of the bounds depending on its sign. In that case, the decision regarding detection would rely on whether the signal falls within the spread of the confidence interval. However, because the spreads (standard deviations) of each variable are different, we would have to adjust the confidence interval limits for each variable, which would make the figure more difficult to interpret. The current approach simplifies the interpretation of the figure by allowing for a quick assessment on whether the bars cross or not the x axis.

3.3 Defining the underlying climate variability noise

Two methods were used for defining internal climate variability:

a) *Preindustrial control runs (piCONTROL)*: Only climate model data were included in this analysis. These models represent downscaled climate model simulations with pre-industrial (1850) greenhouse gas levels fixed. Data is available for each model over a 500-year period. For the 10 models listed in Table S1, the distribution of the *possible* 466 34-year trends (corresponding to the 1983 to 2016 length) constitutes the noise for each model. The 466 34-year trends that make up the noise distributionare calculated by starting at model year 1 and ending at model year 34, then moving one year forward to calculate the trend from model year 2 to model year 35, and continuing this proces until the last trend is computed from model year 467 to model year 500. Note that, due to data availability, for each downscaled GCM we just have one ensemble member, which may lead to an underestimation of the internal climate variability for that model.

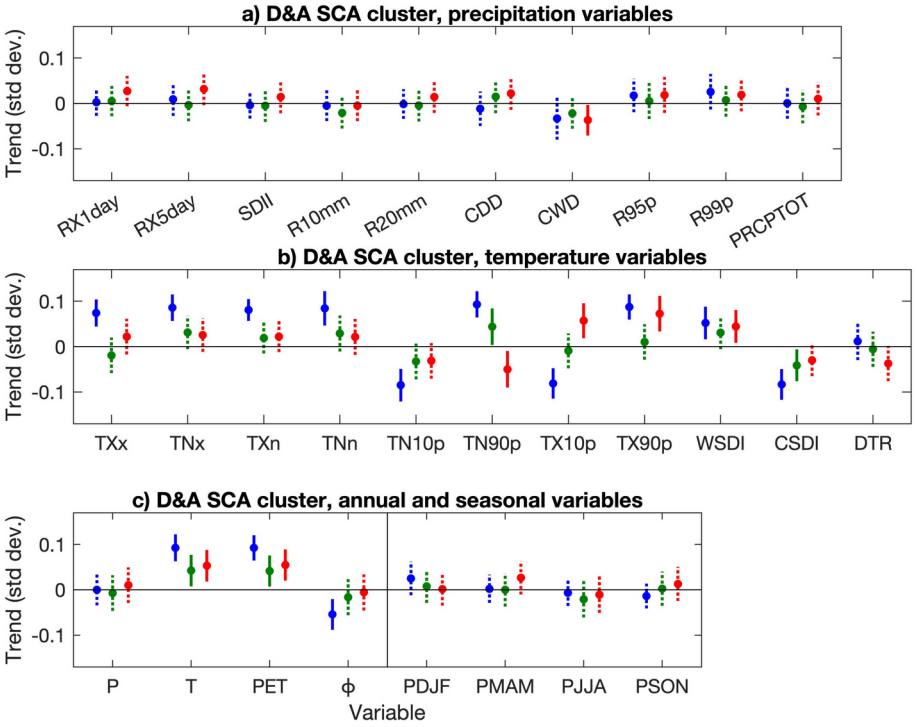

Fig. 2 Results of detection and attribution analysis for the Southern Central America cluster (SCA; see Fig. 1). The analysis was performed for precipitation (top panel) and temperature (middle panel) CLIMDEX extreme indices (definitions in tables S2 and S3 in the Supplementary Information). Also shown in the bottom panel are the analysis for the annual averages of precipitation (P), 2-m temperature (T), potential evapotranspiration (PET) and the ϕ aridity index (defined as P/PET). The four rightmost variables in the bottom panel display the trends of the boreal seasonal precipitation averages. Blue dots represent trends in each standardized variables from a historical run involving an ensemble of 10 models, while the blue confidence intervals are constructed based on the ensemble noise derived from the respective preindustrial control runs. Green dots represent trends based on W5E5 data, with their confidence intervals computed using the synthetic generation described by McKinnon and Deser (2021). Red dots represent trends from the CHIRPs and CHIRTs "observations" (Funk et al. 2015), with the noise levels matching the green methodology. Trends that can (cannot) be detected from the natural variability noise are shown with solid (dotted lines), according to the different methods applied. The trends correspond to the period 1983–2016 for the blue and red analysis, and from 1979 to 2019 for the green analysis

b) *Synthetic generation using climate modes* (McKinnon and Deser 2021; Anderson et al. 2023): Only surface observations and satellite data were used in this method of synthetic generation. We adopt the Observational Large Ensemble (OLEns) method originally developed by McKinnon et al. (2017). Using historical observations as the base for a statistical model, the OLEns preserves characteristics of regional climate that general circulation models may not represent and provides a complement to large ensemble climate models for evaluating internal variability (McKinnon and Deser 2018, 2021; McKinnon et al. 2017). This method assumes that the teleconnection patterns and variability are stationary throughout the whole record. For our application, the procedure starts by fitting a multiple linear regression model for each variable of interest (see McKinnon and Deser (2021) and Anderson et al. (2023)):

$$Y^{i,t} = \beta_o^i + \beta_1^i Niño3.4^t + \beta_2^i CLLJ^t + \beta_3^i PDOperp^t + \beta_4^i Ft^t + \epsilon^{i,t} \quad (2)$$

Where:

$Y^{i,t}$: Each of the 29 variables mentioned in Section 3.1 for cluster *i* and *t* corresponds to the years from 1983 to 2016.

β_k^i: Each of the *k* regression coefficients to be fitted, where k= 0,1,..4 for cluster i.

Niño3.4^t*, CLLJ*^{t}*, PDOperp*^{t}: each of the climate modes defined in the Data section averaged annually for the extreme's indices and the annual indices; and averaged over the respective season for the precipitation seasonal indices.

Ft^t: Anthropogenic forcing representation indexed as low-pass GMT index as explained in the Data section. The time averaging procedure is the same as with the climate modes.

$\epsilon^{i,t}$: Remaining internal variability noise from the regression.

All regressions were fitted over the 1983 to 2016 period, except for the PDJF that was fitted over the period 1984 to 2016 because the DJF season combines two consecutive years. Visual inspection of their histograms revealed that most were normally distributed, except for five precipitation indices across different clusters: R10 mm (BYP cluster), R20 mm (CCS cluster), CDD (WCH cluster), CWD (NP cluster) and R95p (SCA cluster), this indicates a limitation in the interpretation of the results for those variables and clusters. Visual inspection of the residuals did not show any appreciable trend or traces of heteroskedasticity.

The choice of predictors is limited by the length of our data records. While there is some evidence that the Atlantic Multidecadal Oscillation (Enfield et al. 2001) and TNA (Enfield et al. 1999) influence Central American climate, both are dominated by a monotonic trend from 1983–2016 that cannot be statistically distinguished from Ft. As a result, it is possible that the model underestimates multi-decadal variability, that would instead be captured in the regression coefficient for Ft. The incorporation of the Atlantic predictors can overestimate the multidecadal influence (Figures S1 and S2). Also, the Atlantic/Caribbean coefficients were generally smaller as the ones for ENSO and PDO when estimated using a longer record of monthly data (T. Anderson, personal communication), giving us confidence that leaving out the Atlantic influence in Eq. 2 would not represent a major omission.

Similar to McKinnon and Deser (2021) and Anderson et al. (2023), 1000 synthetic simulations from 1900 to 2022 of the climate modes *Niño3.4*^{t}*, CLLJ*^{t} and *PDOperp*^{t} were produced using an Iterative Amplitude Adjusted Fourier Transform (IAAFT) method that retains the original amplitude distributions and power spectra (Schreiber and Schmitz 1996). The IAAFT method does not preserve correlations or coherences between modes, which were generally not found to be meaningful in McKinnon and Deser (2021) and Anderson et al. (2023) once the PDO is orthogonalized with respect to ENSO. The synthetic residual noise $\epsilon^{i,t}$ fields are generated through a block-bootstrapping approach, where the fields are resampled with replacement using a multiyear block size following Wilks (1997), allowing the OLEns to maintain a similar temporal autocorrelation to the original data. Following McKinnon and Deser (2021), we use the 97 th percentile of all estimated block sizes for calculations to preserve the spatial correlation structure of the data; the block sizes in our study are 4 years. The synthetic climate mode time series and residual fields are then linearly combined using the fitted β_k^i s of Eq. 2 to produce pseudo-climate histories of the original climate variables from 1900 to 2022. Note that the bootstrapped epsilon values are from the residuals estimated using a much shorter time series (e.g. 1983–2016 for the daily values). Our full OLEns repeat this process 1,000 times. Note that in Eq. 2 the Ft is used to

take into consideration the forced component and not affecting the other natural modes, in the synthetic generation of the variables, the *Ft* term is not included, because the noise is desired to contain only the natural variability. Therefore, there are 89,000 trends of 34-years to constitute the noise using this procedure.

4 Results

Figure 1 shows the results of the cluster analysis of the annual CLIMDEX extreme indices variables constructed from daily P, Tx and Tn data (Tables S2 and S3 of the Supplementary Information), and annual averages of P, T, PET and the ϕ aridity index from 1983 to 2016. Standardized versions of all those variables were included in the clustering algorithm to identify different subregions. While Central America features a spatial and seasonal precipitation regionalization mentioned in other clustering studies (Alfaro and Cid 1999; Alfaro and Soley 2001; Guillén-Oviedo et al. 2020; Maldonado et al. 2021; Alfaro-Cordoba et al. 2024) and by weather type analysis (Saenz et al. 2023; 2024) that basically responds to the differing ENSO influence on the Pacific and Caribbean slopes, the division presented here does not necessarily resemble the results of those previous studies. Instead, this study reveals additional clusters and regions that represent smaller-scale processes affecting a broader range of extreme events and annual variables. For a depiction of the seasonal cycles of precipitation and temperature in the clusters and a discussion, see Figures S3 and S4 of the Supplementary Information.

In Fig. 2, we present the detection and attribution of the SCA cluster as an example. Results for the other clusters can be found in Figs. 3 and 4 and S5 to S6, and the fitting coefficients of Eq. 2 are provided in Table S4 of the Supplementary Information. When interpreting these figures, the following aspects should be considered:

a) The blue colors represent the analyses of historical (signal) data and the piCONTROL (noise) runs from the ensemble of the 10 ISIMIP3 models listed in Table S1. This part of the analysis is entirely based on GCM data. The green colors indicate the signal from W5E5 dataset, with the noise computed using the synthetic method. Finally, the red colors represent the combination of the trends from observed CHIRPs and CHIRTs, white noise being the same as the one used in the green analysis. It is important to note that this part of the analysis does not include model data.
b) The x axis shows the variable names, while the y axis shows the trends of the standardized variables using the three alternative methodologies for calculating the signals and noises.
c) The dot symbols represent the standardized trends for all the variables computed from the P, Tx and Tn data during the historical (1983–2016) period (1979–2019 for the green analysis). This includes the ensemble of the 10 CMIP6/ISIMIP GCMs from the historical run (blue color), the W5E5 data (green colors) and the trends derived from CHIRPs and CHIRTs data (red color).
d) The bars, centered on the dots, represent the 95% confidence intervals of the trends derived from the noise computed using the three different signal/noise methods. This approach ensures that all methods convey the same message: if the bars intersect the zero line, it indicates that, at the 95% confidence level, the trend of that variable can be

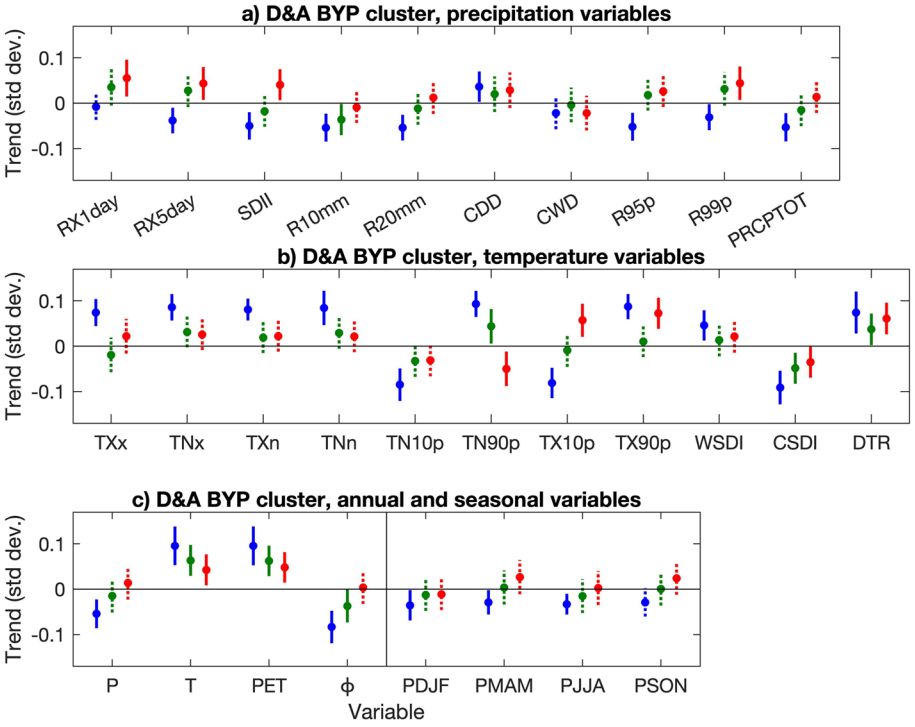

Fig. 3 Same as in Fig. 2 but for the BYP cluster

attributed to natural variability (illustrated with a dashed line). Conversely, if the lines do not cross the zero line (represented with solid lines), there is a 95% confidence that the trend cannot be explained solely by natural variability. However, in the context of multiple hypothesis testing, there is always the possibility of encountering false discovery rates due to chance. Therefore, it is essential to control for the false discovery rate (FDR), that provides a smaller cutoff value to the probabilities above which "discoveries" can be really found. We implemented this control on the results for all clusters in Table 1.

When at least one of the methods detected climate change, we considered that there is a *possible* detection. If all three methods show no detection, then no detection is confirmed. The detection is based on the 1983–2016 (1979–2019 for the green analysis) mean estimate of the trend (as indicated by the dots in the graph), as well as the width of the bars. Since each method yields similar bar length, the differences generally reflect variations in the trend estimates of the signals. The results of the detection analysis is presented in Table 1. A control for FDR at the 0.05 level was included in these results. This means that, on average, no more than 5% of the climate change detections would be false across all 290 hypothesis tests conducted.

There is a consistent lack of detection across the three methodologies regarding precipitation extreme indices in South Central America (SCA), and for the variables P, PDJF, PJJA, and PSON. No detection was found also for variables CWD and PSON in BYP, as well as

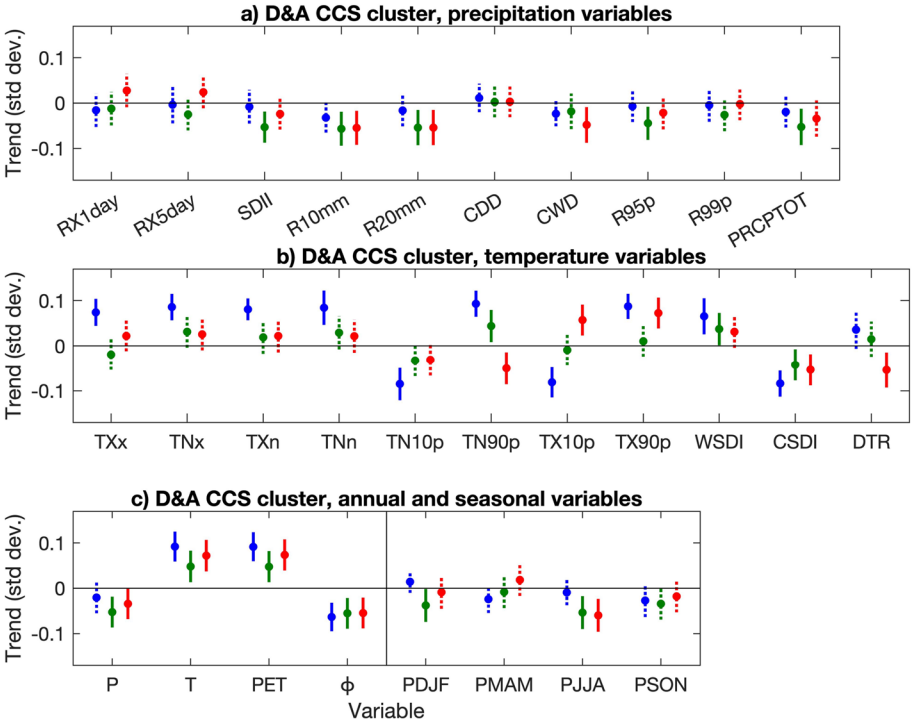

Fig. 4 Same as in Fig. 2 but for the CCS cluster

RX1 day, RX5 day, R95p, R99p, CWD, PSON and PJJA in cluster NP. In the WCH cluster no detection occurred for RX5 day, CWD, R95p, R99p, PDJF, PMAM, and PSON. The CCS cluster showed no detection for variables R20 mm, CWD, R95p, PDJF, PMAM, and PSON, and *possible* detection generally toward drier and warmer environments were detected in the rest of the variables in at least one of the methodologies. The human fingerprint toward warmer and drier environments is evident in T, PET, and TN90p in all clusters. This finding is the most consistent signal among all methodologies. Notably, the detection of drier conditions in annual and seasonal precipitation was mainly observed in northern Caribbean clusters. It should be noted that the residuals for some clusters were previously identified as not being normally distributed. This suggests limitations in interpretating results from both the hybrid methodology and the observation-based method.

5 Discussion and conclusions

We investigated the detection and attribution of various climate variables related to temperature, precipitation and drought extremes in Central America, which is a prominent hotspot for climate change (Giorgi 2006). The aim of our study was to determine whether the observed changes can be attributed to anthropogenic climate change or if they fall within the range of internal climate variability. Weather and climate extremes are known to be heavily influenced by multiple drivers and teleconnections over different timescales.

Table 1 Summary of the detection of climate change results for different variables and clusters. An "X" denotes variables and clusters where the human signal of climate change is detectable at the 95% confidence level. The sign of the "X" (i.e., + or -) indicates the direction of the trend. Three methods were used for computing the combination of signal and noise: "M" for model-based method," H" for hybrid methodology and "O" for the observation-based method. The FDR control was included in this analysis

Variable	CLUSTER														
	SCA			BYP			NP			WCH			CCS		
	M	H	O	M	H	O	M	H	O	M	H	O	M	H	O
1) RX1 day						+ X						+ X			
2) RX5 day				-X		+ X						+ X			
3) SDII				-X		+ X								-X	
4) R10 mm				-X	-X		-X			-X				-X	-X
5) R20 mm				-X			-X							-X	-X
6) CDD				+ X			+ X			+ X					
7) CWD															-X
8) R95p				-X										-X	
9) R99p				-X		+ X									
10) PRCPTOT				-X			-X			-X				-X	
11) TXx	+ X	+ X		+ X			+ X			+ X			+ X		
12) TNx	+ X			+ X			+ X			+ X			+ X		
13) TXn	+ X			+ X			+ X			+ X			+ X		
14) TNn	+ X			+ X			+ X			+ X			+ X		
15) TN10p	+ X			-X			-X			-X			-X		
16) TN90p	+ X	+ X	-X	+ X	+ X	-X	+ X	+ X	-X	+ X	+ X	-X	+ X	+ X	-X
17) TX10p	-X		+ X	-X		+ X	-X		+ X	-X		+ X	-X		+ X
18) TX90p	+ X		+ X	+ X		+ X	+ X		+ X	+ X		+ X	+ X		+ X
19) WSDI	+ X		+ X	+ X			+ X		+ X	+ X			+ X	+ X	
20) CSDI	-X	-X		-X	+ X	-X	-X	+ X	-X	-X	+ X		-X	+ X	-X
21) DTR				+ X	+ X	+ X	+ X		+ X	+ X	+ X				-X
22) P				-X			-X			-X				-X	-X
23) T	+ X	+ X	+ X	+ X	+ X	+ X	+ X	+ X	+ X	+ X	+ X	+ X	+ X	+ X	+ X
24) PET	+ X	+ X	+ X	+ X	+ X	+ X	+ X	+ X	+ X	+ X	+ X	+ X	+ X	+ X	+ X
25) ϕ	-X			-X	-X		-X			-X			-X	-X	-X

Table 1 (continued)

Variable	CLUSTER														
	SCA			BYP			NP			WCH			CCS		
	M	H	O	M	H	O	M	H	O	M	H	O	M	H	O
26) PDJF				-X			-X		-X					-X	
27) PMAM				-X			-X		+ X						
28) PJJA				-X						-X				-X	-X
29) PSON															

Of the three methods used to combine the signal with the range of the internal climate variability (GCMs, hybrid and observation-based synthetic reconstruction), the model-based method produced a less conservative outcome, resulting in more detection cases. This was primarily becasue the signal derived from the piCONTROL demonstrated stronger trends compared to the weaker trends observed using W5E5 and CHIR data combined with synthetic noise. Although the GCM-average trends (blue dots) and observed trends (green and red dots) are viewed equivalently, it is important to note that the the green and red analyses contain a greater contribution from internal variability. The difference between models and observations could be due to model overpredicting the forced response or the observations reflecting sampled internal variability that resulted in smaller trends. It should also noted that the period chosen for the green analysis (1979–2019) does not include the most recent years, which featured significant warming (https://wmo.int/news/media-centre/climate-change-indicators-reached-record-levels-2023-wmo). Nonetheless, our analysis indicate a possible detection of climate change derived from model data, and to a lesser extent from the other methods, particularly concerning temperature extreme indices and precipitation in the northern Caribbean clusters.

The subregions identified through cluster analysis in the northern part of our study region show possible changes toward lower precipitation extremes, alongside overall annual reductions. This finding agrees with previous research suggesting a drier future for this subregion (Hidalgo et al. 2013, 2017). Northern drying in Central America has been linked to both current and future mechanisms, such as a southern shift of the Intertropical Convergence Zone (Rauscher et al. 2008; Hidalgo et al. 2017).

It is evident that warming has led to detectable temperature extremes throughout the region, which could have profound impacts on human lives and environmental systems. It is concerning that areas characterized by higher climatological dryness, warmth and aridity—especially in the CADC—are reporting changes toward greater aridity beyond what is expected from natural climate variability alone. Longer warm spells may adversely affect human health, biodiversity, agriculture, energy production, and various other sectors. Detection of precipitation-related trends were generally found in the northern clusters, which is consistent with findings by Pascale et al. (2021 regarding the difficulty of detecting precipitation trends in Central America.

Overall, our results show that all clusters experienced *possible* positive detection in annual temperature, potential evapotranspiration, and aridity across most temperature extreme variables, while trend detections for extreme, annual and seasonal precipitation were mostly limited to northern clusters. Positive detection of annual temperature for all clusters and of annual potential evapotranspiration in all clusters are consistent with the strong and widespread trends reported in other studies using both station and gridded data (Hidalgo et al. 2017; 2019; Alfaro-Córdoba et al. 2020). The potential evapotranspiration, computed using the Thornthwaite formula, is highly sensitive to temperature, which likely drives the potential detection of this variable, and to a lesser extent, of the aridity index ϕ. In the CADC, the increase in aridity could have significant social impacts on an already vulnerable subregion.

Since there may already be an anthropogenic signal affecting climate extremes is Central America– particularly concerning warming and drying trends in northern clusters—further research should focus on these subregions, to assess potential impacts on human and environmental systems comprehensively. Additionally, a more detailed exploration of issues

related to aridity and drought is needed, including studies to identify the most suitable index for aridity that encompasses the true implications for vegetation and surface water resources limitations.

Supplementary Information The online version contains supplementary material available at https://doi.org/10.1007/s10584-025-03940-5.

Acknowledgements This work was produced when HH was on sabbatical leave from UCR during the year 2024. HH, EA and ER thanks the UCR School of Physics for giving us the research time to develop this study. Thanks to Andrés Gamboa Chacón for assistance with the references of the manuscript. We thank Geog. Marco Acosta for the preparation of the map of Fig. 1.

Author contributions All authors contributed to the study conception and design. Material preparation, data collection and analysis were performed by Hugo G. Hidalgo, Shu Wei Chou Chen and Karen A. McKinnon. The first draft of the manuscript was written by Hugo H. Hidalgo and all authors commented on previous versions of the manuscript. All authors read and approved the final manuscript.

Funding HH, EA and ER wish to acknowledge partial funding for this study through the following Vicerrectoría de Investigación, Universidad de Costa Rica grants: B9454 (supported by Fondo de Grupos), C2103, C30709, C3991 (UCREA), A4906 (PESCTMA) and B0 - 810. EA, and HH were partially supported by a grant awarded by the International Development Research Centre (IDRC), Ottawa, Canada, and the Central American University Council (CSUCA-SICA) to the Red Centroamericana de Ciencias sobre Cambio Climático (RC4) project (CR- 66, C4468, SIA 0054–2, the opinions expressed here do not necessarily represent those of IDRC, CSUCA, or the Board of Governors). KM was supported by the Packard Foundation. TN was supported by JSPS KAKENHI Grant Number 23 KK0077.

Data availability All original datasets are available freely from the original sources as stated in the Data section. Processed data from the article are available in the repository kerwa.ucr.ac.cr of the University of Costa Rica (https://hdl.handle.net/10669/91762).

Declarations

Competing interests The authors have no competing interests to declare that are relevant to the content of this article.

References

Aguilar E, Peterson TC, Ramírez Obando P et al (2005) Changes in precipitation and temperature extremes in Central America and northern South America, 1961–2003. J Geophys Res: Atmos 110:2005JD006119. https://doi.org/10.1029/2005JD006119

Alfaro EJ, Cid Serrano LR (1999) Ajuste de un modelo VARMA para los campos de anomalías de precipitación en Centroamérica y los índices de los océanos Pacífico y Atlántico Tropical. Atmósfera 12:205–222. https://hdl.handle.net/10669/15236

Alfaro EJ, Soley FJ (2001) Ajuste de un modelo VAR como predictor de los campos de anomalías de precipitación en Centroamérica. Revista De Matemática: Teoría y Aplicaciones 8:96–116. https://doi.org/10.15517/rmta.v8i1.199

Alfaro E, Hidalgo H, Mora N (2016) Prediction of MJ rainfall season using CCA models. Tópicos Meteorológicos y Oceanográficos 15(2):5–19. https://hdl.handle.net/10669/76126

Alfaro-Córdoba M, Hidalgo HG, Alfaro EJ (2020) Aridity Trends in Central America: A Spatial Correlation Analysis. Atmosphere 11:427. https://doi.org/10.3390/atmos11040427

Alfaro-Córdoba M, Mora-Sandí NP, Hidalgo HG, Alfaro EJ (2024) Central American climate extreme trends: A statistical analysis of CLIMDEX indices. Int J Climatol joc.8571. https://doi.org/10.1002/joc.8571

Amador AJA (1998) A climatic feature of the tropical Americas: the trade wind easterly jet. Revista Tópicos Meteorológicos y Oceanográficos 5(2):91–102. https://hdl.handle.net/10669/76623

Amador Astúa AJA (2008) The Intra-Americas sea low-level Jet: overview and future research. Ann NY Acad Sci 1146:153–188. https://doi.org/10.1196/annals.1446.012

Amador AJA, Maldonado Mora TJ, Rivera Fernández E et al (2018) La Corriente en Chorro del Caribe: Observaciones, modelado multifísica, interacciones multiescala e impacto regional. San José, Costa Rica: Universidad de Costa Rica. https://hdl.handle.net/10669/77383

Anderson TG, Anchukaitis KJ, Pons D, Taylor M (2019) Multiscale trends and precipitation extremes in the Central American midsummer drought. Environ Res Lett 14:124016. https://doi.org/10.1088/1748-9326/ab5023

Anderson TG, McKinnon KA, Pons D, Anchukaitis KJ (2023) How exceptional was the 2015–2019 Central American drought? Geophysical Research Letters 50:e2023GL105391. https://doi.org/10.1029/2023GL105391

Angeles-Malaspina M, González-Cruz JE, Ramírez-Beltran N (2018) Projections of heat waves events in the Intra-Americas region using multimodel ensemble. Adv Meteorol 2018:1–16. https://doi.org/10.1155/2018/7827984

Arias PA, Bellouin N, Coppola E, Jones RG et al (2021) Technical summary. Climate change 2021: the physical science basis. contribution of working group I to the sixth assessment report of the intergovernmental panel on climate change [Masson-Delmotte V, Zhai P, Pirani A, Connors SL, Péan C, Berger S, Caud N, Chen Y, Goldfarb L, Gomis MI, Huang M, Leitzell K, Lonnoy E, Matthews JBR, Maycock TK, Waterfield T, Yelekçi O, Yu R, Zhou B (eds.)]. Cambridge University Press. Cambridge, United Kingdom and New York, NY, USA, pp 33−144. https://doi.org/10.1017/9781009157896.002

Baker A (2023) Chronic kidney disease is poised to become the black lung of climate change. In: TIME. https://time.com/6303020/chronic-kidney-disease-climate-change/. Accessed 1/1/2023

Cavazos T, Bettolli ML, Campbell D et al (2024) Challenges for climate change adaptation in Latin America and the Caribbean region. Front Clim 6:1392033. https://doi.org/10.3389/fclim.2024.1392033

Centella-Artola A, Bezanilla-Morlot A, Taylor MA et al (2020) Evaluation of sixteen gridded precipitation datasets over the caribbean region using gauge observations. Atmosphere 11:1334. https://doi.org/10.3390/atmos11121334

Cucchi M, Weedon GP, Amici A et al (2020) WFDE5: bias-adjusted ERA5 reanalysis data for impact studies. Earth System Science Data 12:2097–2120. https://doi.org/10.5194/essd-12-2097-2020

Donatti CI, Nicholas K, Fedele G et al (2024) Global hotspots of climate-related disasters. Int J Disaster Risk Reduction 108:104488. https://doi.org/10.1016/j.ijdrr.2024.104488

Durán-Quesada AM, Sorí R, Ordoñez P, Gimeno L (2020) Climate perspectives in the Intra-Americas seas. Atmosphere 11:959. https://doi.org/10.3390/atmos11090959

Enfield DB, Alfaro EJ (1999) The dependence of Caribbean rainfall on the interaction of the tropical Atlantic and Pacific Oceans. J Clim 12:2093–2103. https://doi.org/10.1175/1520-0442(1999)012/2093:TDOCRO/2.0.CO;2

Enfield DB, Mestas-Nuñez AM, Mayer DA, Cid-Serrano L (1999) How ubiquitous is the dipole relationship in tropical Atlantic Sea surface temperatures? J Geophys Res: Oceans 104:7841–7848. https://doi.org/10.1029/1998JC900109

Enfield DB, Mestas-Nuñez AM, Trimble PJ (2001) The Atlantic multidecadal oscillation and its relation to rainfall and river flows in the continental U.S. Geophys Res Lett 28:2077–2080. https://doi.org/10.1029/2000GL012745

Fuentes-Franco R, Coppola E, Giorgi F et al (2015) Inter-annual variability of precipitation over Southern Mexico and Central America and its relationship to sea surface temperature from a set of future projections from CMIP5 GCMs and RegCM4 CORDEX simulations. Clim Dyn 45:425–440. https://doi.org/10.1007/s00382-014-2258-6

Funk C, Peterson P, Landsfeld M et al (2015) The climate hazards infrared precipitation with stations—a new environmental record for monitoring extremes. Sci Data 2:150066. https://doi.org/10.1038/sdata.2015.66

Funk C, Peterson P, Peterson S et al (2019) A high-resolution 1983–2016 Tmax climate data record based on infrared temperatures and stations by the climate hazard center. J Clim 32:5639–5658. https://doi.org/10.1175/JCLI-D-18-0698.1

García-Franco JL, Chadwick R, Gray L et al (2022) Revisiting mechanisms of the mesoamerican midsummer drought. Clim Dyn 60:549–569. https://doi.org/10.1007/s00382-022-06338-6

Giorgi F (2006) Climate change hot-spots. Geophys Res Lett 33:2006GL025734. https://doi.org/10.1029/2006GL025734

GISTEMP Team (2024) GISS surface temperature analysis (GISTEMP), version 4. NASA Goddard Institute for Space Studies. Dataset Accessed 2024–04–08 at https://data.giss.nasa.gov/gistemp/

González-Trujillo JD, Alagador D, González-del-Pliego P, Araújo MB (2024). Exposure of protected areas in Central America to extreme weather events. Conserv Biol 1–12. https://doi.org/10.1111/cobi.14251

Gotlieb Y, Pérez Briceño PM, Hidalgo León HG, Alfaro Martínez EJ (2019) The Central American dry corridor: a consensus statement and its background. Revista Yu'am 3(5):42–51. https://hdl.handle.net/10669/79953

Guevara-Murua A, Williams CA, Hendy EJ, Imbach P (2018) 300 years of hydrological records and societal responses to droughts and floods on the Pacific coast of Central America. Climate of the past 14(2):175–191. https://doi.org/10.5194/cp-14-175-2018

Guillén-Oviedo HS, Cid-Serrano LR, Alfaro-Martínez EJ (2020) Comparison of parameters of the generalized extreme value distribution associated with extreme rainfall events in Central America. Revista Uniciencia 34:111–128. https://doi.org/10.15359/ru.34-1.7

Hawkins E, Frame D, Harrington L et al (2020) Observed Emergence of the Climate Change Signal: From the Familiar to the Unknown. Geophysical Research Letters 47:e2019GL086259. https://doi.org/10.1029/2019GL086259

Held IM, Soden BJ (2006) Robust responses of the hydrological cycle to global warming. J Clim 19:5686–5699. https://doi.org/10.1175/JCLI3990.1

Hersbach H, Bell B, Berrisford P et al (2020) The ERA5 global reanalysis. Q J R Meteorol Soc 146:1999–2049. https://doi.org/10.1002/qj.3803

Hidalgo HG, Amador JA, Alfaro EJ, Quesada B (2013) Hydrological climate change projections for Central America. J Hydrol 495:94–112. https://doi.org/10.1016/j.jhydrol.2013.05.004

Hidalgo HG, Durán-quesada AM, Amador JA, Alfaro EJ (2015) The Caribbean low-level jet, the inter-tropical convergence zone and precipitation patterns in the intra-americas sea: a proposed dynamical mechanism. Geogr Ann Ser B 97:41–59. https://doi.org/10.1111/geoa.12085

Hidalgo HG, Alfaro EJ, Quesada-Montano B (2017) Observed (1970–1999) climate variability in Central America using a high-resolution meteorological dataset with implication to climate change studies. Clim Change 141:13–28. https://doi.org/10.1007/s10584-016-1786-y

Hidalgo HG, Alfaro EJ, Amador JA, Bastidas Á (2019) Precursors of quasi-decadal dry-spells in the Central America Dry Corridor. Clim Dyn 53:1307–1322. https://doi.org/10.1007/s00382-019-04638-y

Hyun S, Yeh S, Song S et al (2020) Understanding Intermodel Diversity When Simulating the Time of Emergence in CMIP5 Climate Models. Geophys Res Lett 47:e2020GL087923. https://doi.org/10.1029/2020GL087923

Kalnay E, Kanamitsu M, Kistler R et al (1996) The NCEP/NCAR 40-year reanalysis project. Bull Am Meteor Soc 77:437–471. https://doi.org/10.1175/1520-0477(1996)077/0437:TNYRP/2.0.CO;2

Kawase H, Nosaka M, Watanabe SI et al (2023) Identifying robust changes of extreme precipitation in Japan from large ensemble 5-km-grid regional experiments for 4K warming scenario. J Geophys Res: Atmos 128:e2023JD038513. https://doi.org/10.1029/2023JD038513

Lange S (2019) Trend-preserving bias adjustment and statistical downscaling with ISIMIP3BASD (v1.0). Geosci Model Dev 12:3055–3070. https://doi.org/10.5194/gmd-12-3055-2019

Lange S (2022) ISIMIP3BASD. Version 2.5.2. Zenodo. https://zenodo.org/record/6344911

Lange S, Büchner M (2021) ISIMIP3b bias-adjusted atmospheric climate input data. https://doi.org/10.48364/ISIMIP.842396.1. Accessed 1/9/2024

Lange S, Menz C, Gleixner S et al (2021) WFDE5 over land merged with ERA5 over the ocean (W5E5 v2.0). https://doi.org/10.48364/ISIMIP.342217

Lange S, Mengel M, Treu S, Büchner M (2023a) ISIMIP3a atmospheric climate input data. https://doi.org/10.48364/ISIMIP.982724.2

Lange S, Quesada-Chacón D, Büchner M (2023b) Secondary ISIMIP3b bias-adjusted atmospheric climate input data. https://doi.org/10.48364/ISIMIP.581124.3

Lenssen N, Schmidt G, Hansen J, Menne M, Persin A, Ruedy R, Zyss D (2019) Improvements in the GISTEMP uncertainty model. J Geophys Res: Atmos 124(12):6307–6326. https://doi.org/10.1029/2018JD029522

Ley D, Guillén Bolaños T, Castaneda A et al (2023) Central America urgently needs to reduce the growing adaptation gap to climate change. Front Clim 5. https://doi.org/10.3389/fclim.2023.1215062

Magaña V, Amador JA, Medina S (1999) The midsummer drought over Mexico and Central America. J Clim 12:1577–1588. https://doi.org/10.1175/1520-0442(1999)012/1577:TMDOMA/2.0.CO;2
Maldonado T, Alfaro E, Rutgersson A, Amador JA (2017) The early rainy season in Central America: the role of the tropical North Atlantic SSTs. Int J Climatol 37:3731–3742. https://doi.org/10.1002/joc.4958
Maldonado T, Alfaro EJ, Hidalgo HG (2018) A review of the main drivers and variability of Central America's Climate and seasonal forecast systems. Revista de Biología Tropical 66:153–175. https://doi.org/10.15517/rbt.v66i1.33294
Maldonado T, Alfaro EJ, Hidalgo HG (2021) Análisis de los conglomerados de precipitación y sus cambios estacionales sobre América Central para el período 1976–2015. Revista de Matemática: Teoría y Aplicaciones 28:337–362. https://doi.org/10.15517/rmta.v28i2.42322
Mantua NJ, Hare SR, Zhang Y et al (1997) A pacific interdecadal climate oscillation with impacts on salmon production. Bull Am Meteor Soc 78:1069–1079. https://doi.org/10.1175/1520-0477(1997)078/1069:APICOW/2.0.CO;2
McKinnon KA, Deser C (2018) Internal variability and regional climate trends in an observational large ensemble. J Clim 31:6783–6802. https://doi.org/10.1175/JCLI-D-17-0901.1
McKinnon KA, Poppick A, Dunn-Sigouin E, Deser C (2017) An "Observational Large Ensemble" to compare observed and modeled temperature trend uncertainty due to internal variability. J Clim 30:7585–7598. https://doi.org/10.1175/JCLI-D-16-0905.1
McKinnon KA, Deser C (2021) The inherent uncertainty of precipitation variability, trends, and extremes due to internal variability, with implications for Western US water resources. J Clim 1–46. https://doi.org/10.1175/JCLI-D-21-0251.1
Miranda-Chacón Z, Alfaro-Martínez EJ, Hidalgo-León HG, Arguedas-Ramírez G, Rivera-Chavarría AL (2023) Policy brief for Costa Rica 2023. The lancet countdown on health and climate change. https://doi.org/lancetcountdown.org. Accessed 1/9/2024
Morataya-Montenegro R, Bautista-Solís P (2020) Water governance and adaptation to drought in Guanacaste, Costa Rica. In: Vieira E, Sandoval-Solis S, Pedrosa V, Ortiz-Partida J (eds) Integrated Water Resource Management. Springer, Cham. https://doi.org/10.1007/978-3-030-16565-9_8
Nakaegawa T, Murazaki K (2022) Historical trends in climate indices relevant to surface air temperature and precipitation in Japan for recent 120 years. Int J Climatol 42:8950–8970. https://doi.org/10.1002/joc.7784
Neelin JD, Münnich M, Su H et al (2006) Tropical drying trends in global warming models and observations. Proc Natl Acad Sci 103:6110–6115. https://doi.org/10.1073/pnas.0601798103
Pascale S, Carvalho LMV, Adams DK et al (2019) Current and future variations of the monsoons of the Americas in a warming climate. Curr Clim Change Rep 5:125–144. https://doi.org/10.1007/s40641-019-00135-w
Pascale S, Kapnick SB, Delworth TL et al (2021) Natural variability vs forced signal in the 2015–2019 Central American drought. Clim Change 168:16. https://doi.org/10.1007/s10584-021-03228-4
Pérez Briceño PM, Alfaro Martínez EJ, Hidalgo León HG, Jiménez F (2016) Distribución espacial de impactos de eventos hidrometeorológicos en América Central. Rev Climatol 16:63–75. https://hdl.handle.net/10669/74079
Perkins-Kirkpatrick S, Barriopedro D, Jha R et al (2024) Extreme terrestrial heat in 2023. Nat Rev Earth Environ 5:244–246. https://doi.org/10.1038/s43017-024-00536-y
Quesada-Hernández LE, Calvo-Solano OD, Hidalgo HG et al (2019) Dynamical delimitation of the Central American Dry Corridor (CADC) using drought indices and aridity values. Prog Phys Geogr: Earth Environ 43:627–642. https://doi.org/10.1177/0309133319860224
Ramirez-Beltran ND, Gonzalez JE, Castro JM et al (2017) Analysis of the heat index in the mesoamerica and caribbean region. J Appl Meteorol Climatol 56:2905–2925. https://doi.org/10.1175/JAMC-D-16-0167.1
Rauscher SA, Giorgi F, Diffenbaugh NS, Seth A (2008) Extension and Intensification of the Meso-American mid-summer drought in the twenty-first century. Clim Dyn 31:551–571. https://doi.org/10.1007/s00382-007-0359-1
Romero D, Alfaro EJ (2024) Spatiotemporal variability of the rainy season in the Yucatan Peninsula. Int J Climatol 44:2561–2574. https://doi.org/10.1002/joc.8468
Sáenz F, Hidalgo HG, Muñoz ÁG et al (2023) Atmospheric circulation types controlling rainfall in the Central American Isthmus. Int J Climatol 43:197–218. https://doi.org/10.1002/joc.7745
Sáenz SF, Alfaro EJ, Hidalgo HG (2024) Weather types for the seasonal transitions in Central America. Revista De Matemática: Teoría y Aplicaciones 31:27–56. https://doi.org/10.15517/rmta.v31i1.54869
Schreiber T, Schmitz A (1996) Improved surrogate data for nonlinearity tests. Phys Rev Lett 77:635–638. https://doi.org/10.1103/PhysRevLett.77.635

Seneviratne SI, Zhang X, Adnan M et al (2021) Weather and climate extreme events in a changing climate. Climate change 2021: the physical science basis. Contribution of working group I to the sixth assessment report of the intergovernmental panel on climate change [Masson-Delmotte V, Zhai P, Pirani A, Connors SL, Péan C, Berger S, Caud N, Chen Y, Goldfarb L, Gomis MI, Huang M, Leitzell K, Lonnoy E, Matthews JBR, Maycock TK, Waterfield T, Yelekçi O, Yu R, Zhou B (eds.)]. Cambridge University Press. Cambridge, United Kingdom and New York, NY, USA, pp 1513–1766. https://doi.org/10.1017/9781009157896.013

Stewart IT, Maurer EP, Stahl K, Joseph K (2021) Recent evidence for warmer and drier growing seasons in climate sensitive regions of Central America from multiple global datasets. Int J Climatol 42:1399–1417. https://doi.org/10.1002/joc.7310

Thornthwaite CW (1948) An Approach toward a Rational Classification of Climate. Geogr Rev 38:55. https://doi.org/10.2307/210739

Trenberth KE, Dai A, Rasmussen RM, Parsons DB (2003) The changing character of precipitation. Bull Am Meteor Soc 84:1205–1218. https://doi.org/10.1175/BAMS-84-9-1205

Ugalde KC (2022) Estudio del inicio y término de la estación lluviosa en el Pacífico Norte de Costa Rica en el periodo 1950–2020. Universidad de Costa Rica, San José, Costa Rica

Wang C (2007) Variability of the Caribbean low-level jet and its relations to climate. Clim Dyn 29:411–422. https://doi.org/10.1007/s00382-007-0243-z

Weedon GP, Balsamo G, Bellouin N et al (2014) The WFDEI meteorological forcing data set: WATCH Forcing Data methodology applied to ERA-Interim reanalysis data. Water Resour Res 50:7505–7514. https://doi.org/10.1002/2014WR015638

Wilks DS (1997) Resampling hypothesis tests for autocorrelated fields. J Clim 10:65–82. https://doi.org/10.1175/1520-0442(1997)010/0065:RHTFAF/2.0.CO;2

Wilks DS (2019) Chapter 16, Cluster Analysis. Statistical Methods in the Atmospheric Sciences. 4ta. ed. Elsevier. 721–738. https://doi.org/10.1016/C2017-0-03921-6

Ying J, Collins M, Cai W et al (2022) Emergence of climate change in the tropical Pacific. Nat Clim Chang 12:356–364. https://doi.org/10.1038/s41558-022-01301-z

Authors and Affiliations

H. G. Hidalgo[1] · S. W. Chou-Chen[2] · K. A. McKinnon[3] · S. Pascale[4] · D. Quesada-Chacón[5] · E. J. Alfaro[6] · P. Bautista-Solís[7] · P. M. Pérez-Briceño[8] · H. F. Diaz[9] · T. Maldonado[10] · E. R. Rivera[11] · T. Nakaegawa[12]

✉ H. G. Hidalgo
hugo.hidalgo@ucr.ac.cr

[1] Escuela de Física, Centro de Investigaciones Geofísicas y Centro de Investigación en Matemática Pura y Aplicada, Universidad de Costa Rica, 2060-Ciudad de la Investigación, San José 11501, Costa Rica

[2] Escuela de Estadística, Centro de Investigación en Matemática Pura y Aplicada, Universidad de Costa Rica, San José, Costa Rica

[3] Department of Statistics and Data Science, Department of Atmospheric and Oceanic Sciences, and Institute of the Environment and Sustainability, University of California, Los Angeles, USA

[4] Department of Physics and Astronomy (DIFA), University of Bologna, Bologna, Italy

[5] Potsdam Institute for Climate Impact Research, Potsdam, Germany

[6] Escuela de Física, Centro de Investigaciones Geofísicas y Centro de Investigación en Ciencias del Mar y Limnología, Universidad de Costa Rica, San José, Costa Rica

[7] Universidad Nacional, Centro Mesoamericano de Desarrollo Sostenible del Trópico Seco (Cemede-UNA), Heredia, Costa Rica

[8] Escuela de Geografía, Centro de Investigaciones Geofísicas, Universidad de Costa Rica, San José, Costa Rica

[9] Department of Geography and Environment, University of Hawaii at Manoa, Honolulu, HI, USA

[10] Centro de Investigaciones Geofísicas, Universidad de Costa Rica, San José, Costa Rica

[11] Escuela de Física y Centro de Investigaciones Geofísicas, Universidad de Costa Rica, San José, Costa Rica

[12] Meteorological Research Institute, Tsukuba, Japan

Supplementary information of:
Detection and attribution of trends of meteorological extremes in Central America
Climatic Change

By:

Hidalgo, H.G.; Chou-Chen, S.W.; McKinnon, K. A.; Pascale, S.; Quesada-Chacón, D.; Alfaro, E.J.; Bautista-Solís, P.; Pérez-Briceño, P.M.; Diaz, H.F., Maldonado, T., Rivera, E. R., Nakaegawa, T.

Section 1. Tables of the models used in the study and on the definition of extreme indices of precipitation and temperature calculated from daily precipitation, maximum and minimum data.

Table S1. CMIP6 General Circulation Models (CGMs) used in this analysis.

ID	Model	Climate Center	Run	Native resolution
1	GFDL-ESM4	Geophysical Fluid Dynamics Laboratory (GFDL)	r1i1p1f1	lonlat (288x180)
2	IPSL-CM6A-LR	Institut Pierre-Simon Laplace (IPSL)	r1i1p1f1	lonlat (144x143)
3	MPI-ESM1-2-HR	Max Planck Institute for Meteorology (MPI-M)	r1i1p1f1	gaussian (384x192)
4	MRI-ESM2-0	Meteorological Research Institute (MRI)	r1i1p1f1	gaussian (320x160)
5	UKESM1-0-LL	UK Earth System Modelling	r1i1p1f2	lonlat (192x144)
6	CanESM5	Canadian Centre for Climate Modelling and Analysis (CCCMA)	r1i1p1f1	gaussian (128x64)
7	CNRM-CM6-1	Centre National de Recherches Meteorologiques / Centre 3 Europeen de Recherche et Formation Avancees en Calcul Scientifique (CNRM)	r1i1p1f2	gaussian (256x128)
8	CNRM-ESM2-1	CNRM	r1i1p1f2	gaussian (256x128)
9	EC-Earth3	EC-EARTH consortium	r1i1p1f1	gaussian (512x256)

10	MIROC6	Atmosphere and Ocean Research Institute (The University of 3 Tokyo), National Institute for Environmental Studies, and Japan Agency for Marine-Earth Science and Technology. (MIROC)	r1i1p1f1	gaussian (256x128)

Table S2. List of precipitation indices from CLIMDEX. RR=rainfall rate.

ID	Name	Indicator name	Definition	Units
1	RX1day	max 1-day precipitation amount	annual maximum 1-day precipitation	mm
2	RX5day	max 5-day precipitation amount	annual maximum 5-day precipitation	mm
3	SDII	simple daily intensity index	annual total precipitation divided by the number of wet days in the year	mm/day
4	R10mm	number of heavy precipitation days	annual count of days when precipitation ≥ 10mm	days
5	R20mm	number of very heavy precipitation days	annual count of days when precipitation ≥ 20mm	days
6	CDD	consecutive dry days & maximum number of consecutive days with daily rainfall	maximum number of consecutive days with daily rainfall < 1mm	days
7	CWD	consecutive wet days	maximum number of consecutive days with daily rainfall ≥ 1mm	days
8	R95p	very wet days	annual total PRCP when RR > 95th percentile	mm
9	R99p	extremely wet days	annual total PRCP when RR > 99th percentile	mm

10	PRCPTOT	annual total wet-day precipitation	annual total PRCP in wet days (RR ≥ 1mm)	mm

Table S3. List of temperature indices from CLIMDEX.

ID	Name	Indicator name	Definition	Units
1	TXx	max Tmax	annual maximum value of daily maximum temperature	ºC
2	TNx	max Tmin	annual maximum value of daily minimum temp	ºC
3	TXn	min Tmax	annual minimum value of daily maximum temperature	ºC
4	TNn	min Tmin	annual minimum value of daily minimum temp	ºC
5	TN10p	cool nights	percentage of days when TN < 10th percentile	% days
6	TN90p	warm nights	percentage of days when TN > 90th percentile	% days
7	TX10p	cool days	percentage of days when TX < 10th percentile	% days
8	TX90p	warm days	percentage of days when TX > 90th percentile	% days
9	WSDI	warm spell duration indicator	annual count of days with at least 6 consecutive days when TX > 90th percentile	% days
10	CSDI	cold spell duration indicator	annual count of days with at least 6 consecutive days when TN < 10th percentile	% days
11	DTR	diurnal temperature range	annual mean difference between TX and TN	ºC

Section 2. Examples of the effect on the December-January-February (DJF) precipitation noise traces by fitting equation 3 with different types of Atlantic/Caribbean predictors.

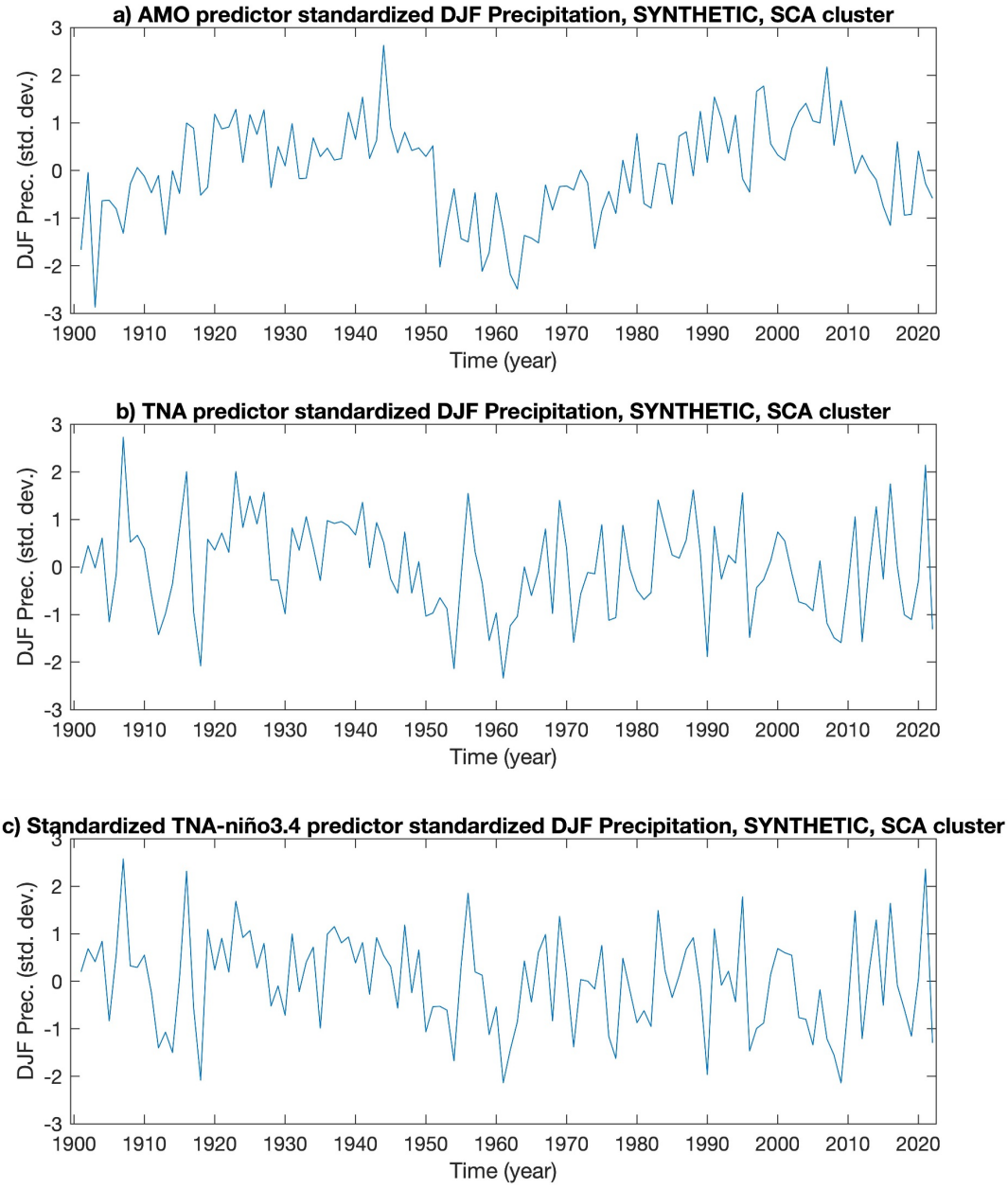

Figure S1. Standardized December-January-February precipitation (PDJF) example traces for three versions of fitting Eq. 3 using Atlantic Multidecadal Oscillation (AMO) (top), Tropical North Atlantic (TNA index) (middle) and a composite index of the difference between standardized versions of the TNA minus niño3.4 datasets. For each of these ways to fit the Eq. 3, 1000 traces of the noise were generated synthetically. Time series shown for the SCP cluster.

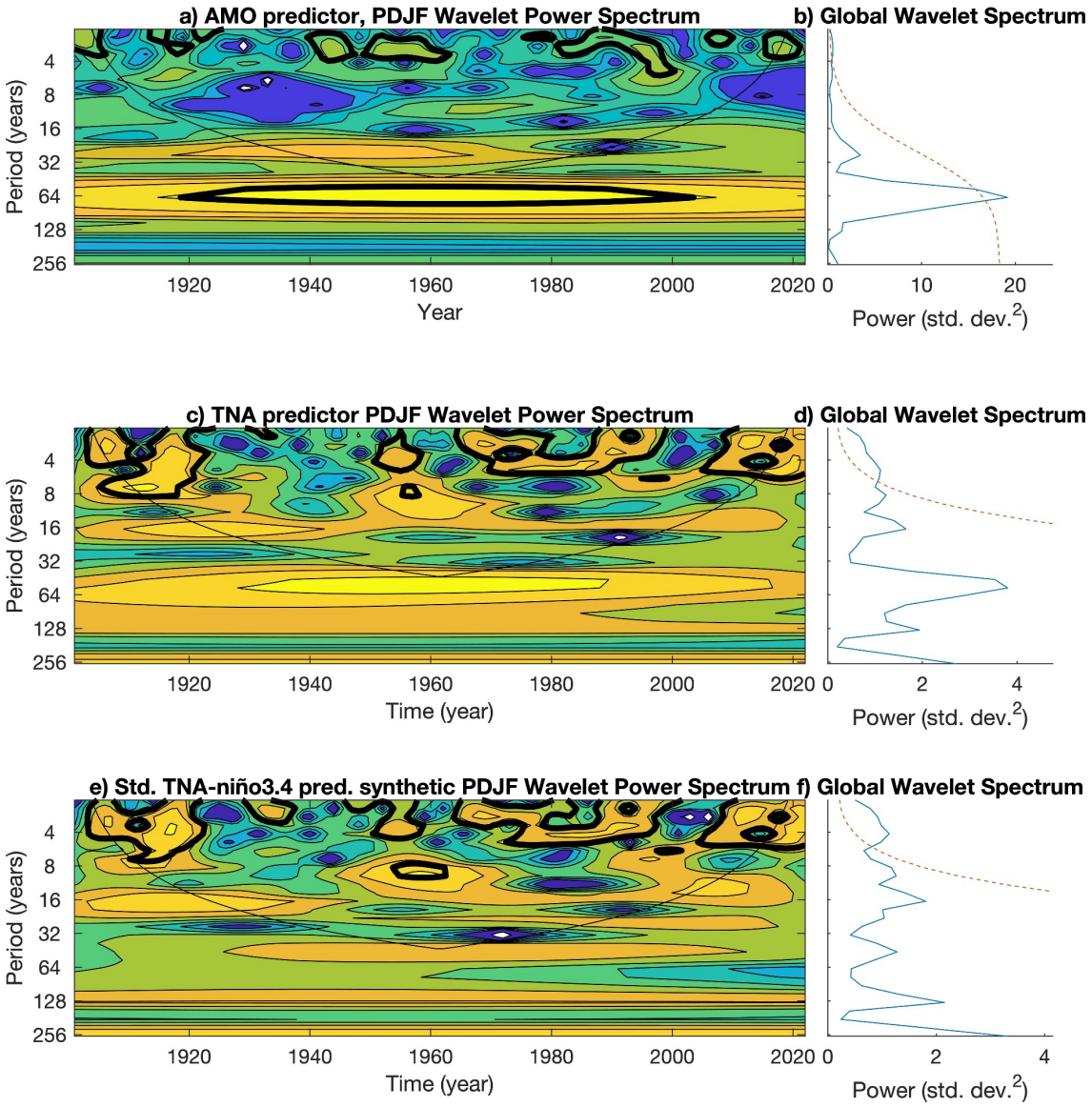

Figure S2. Same as Fig. S1, but for the wavelet power spectrum according to Torrence and Compo (1998). The mother wavelet is Morlet, dt=1, pad=1, dj=0.25, s0=2*dt, j1=7/dj, lag1=0.72. The dark thick lines represent places in the spectrum that are significantly above the red-noise background. The cone of influence below plots (a), (c), and (e) represents frequencies of signals that are by the boundaries of the plot and should be interpreted with caution. The plots on the right represent the global spectrum as an integration of the data for all the times.

Section 3. Precipitation and temperature climatologies of the clusters of Fig. 1.

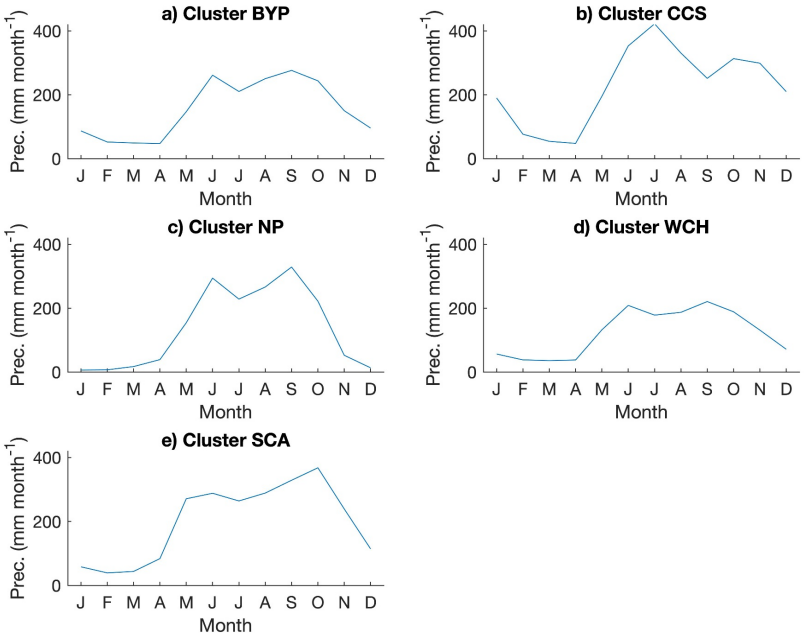

Figure S3. Seasonal cycles of precipitation for the clusters defined in Fig.1.

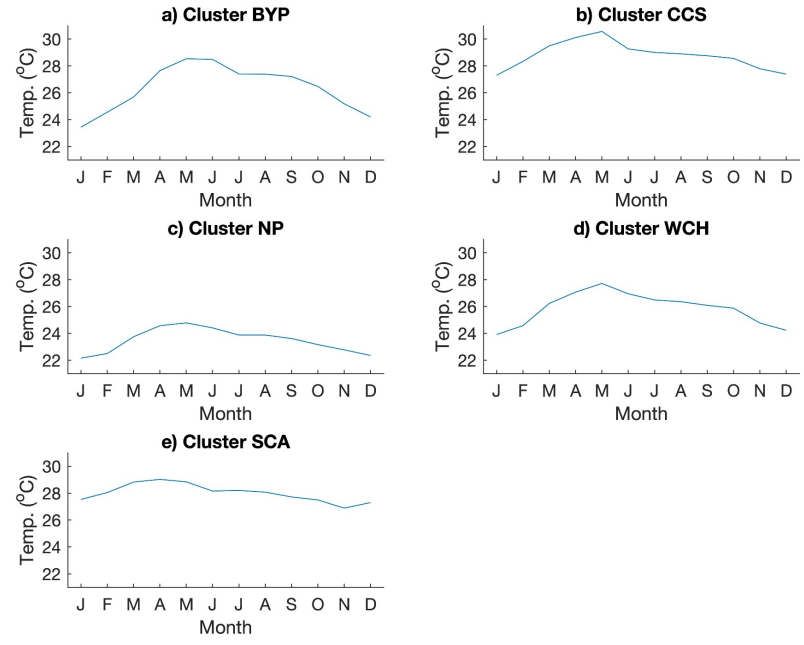

Figure S4. Seasonal cycles of temperature for the clusters defined in Fig.1.

Cluster BYP is similar to WCH in terms of the relative seasonal cycle of precipitation distribution throughout the year, but BYP has more absolute monthly accumulations.during the wet season. BYP is a region where

multiple tropical cyclones from the Caribbean make landfall (more than in WCH) and that may explain a difference in the distribution of extreme precipitation that ultimately is reflected in monthly accumulations. CCS has the wettest month and a remarkable distribution that stands out from the rest (clearly a Caribbean slope type of distribution). NP is the only one with a clear dry season (although other regions may have dry seasons but are averaged with other regions that present significant rainfall from December to March). SCA has an earlier start of the rainy season of all distributions.

Temperature-wise, BYP, CCS and SCA showed the highest temperatures, WCH is moderate and NP is the coldest region. The combination of very hot-wet versus moderate temp-rain may also explain the difference between cluster BYP and WCH.

Section 4. Table of statistics related to the fit of equation 3.

Table S4. Fitting parameters for Eq. 3. See definitions of the variables in tables S2 and S3 and definition of the clusters in Fig. 1.

Variable	Cluster	β_0 *(inter.)*	β_1 *(Niño3.4)*	β_2 *(CLLJ)*	β_3 *(PDO_{perp})*	β_4 *(F_t)*	r^2
RX1day	SCA	-1.36	0.69	-0.03	-0.03	2.75	0.51
	BYP	-1.11	0.55	-0.15	-0.15	2.52	0.38
	NP	-0.65	0.23	0.15	0.15	1.14	0.22
	WCH	-0.78	-0.07	0.31	0.31	1.49	0.17
	CCS	1.25	-0.32	-0.50	-0.50	-2.35	0.62
RX5day	SCA	-0.12	0.69	0.48	0.48	0.02	0.50
	BYP	0.80	-0.36	-0.19	-0.19	-1.44	0.32
	NP	-0.83	0.10	-0.07	-0.07	1.69	0.11
	WCH	0.85	-0.01	-0.74	-0.74	-1.55	0.47
	CCS	-1.86	0.52	0.29	0.29	3.78	0.81
SDII	SCA	-1.15	0.36	0.45	0.45	2.25	0.50
	BYP	-2.09	0.36	-0.14	-0.14	4.32	0.67
	NP	1.25	-0.76	0.18	0.18	-2.58	0.45
	WCH	-1.32	0.50	0.35	0.35	2.72	0.58
	CCS	1.29	-0.50	-0.18	-0.18	-2.53	0.48
R10mm	SCA	1.07	-0.79	-0.22	-0.22	-2.04	0.64
	BYP	-0.63	-0.08	-0.12	-0.12	1.29	0.07
	NP	-1.82	0.66	-0.41	-0.41	3.88	0.59
	WCH	0.59	-0.40	-0.47	-0.47	-0.95	0.43

	CCS	-1.73	0.70	-0.43	-0.43	3.75	0.56
R20mm	SCA	-1.36	0.66	0.27	0.27	2.76	0.65
	BYP	0.75	-0.37	-0.19	-0.19	-1.34	0.30
	NP	1.37	-0.62	-0.16	-0.16	-2.62	0.65
	WCH	-1.73	0.55	-0.17	-0.17	3.61	0.53
	CCS	-1.41	0.10	-0.17	-0.17	3.08	0.27
CDD	SCA	0.53	-0.75	-0.58	-0.58	-0.84	0.73
	BYP	-1.19	0.18	-0.36	-0.36	2.34	0.40
	NP	-2.11	0.59	-0.05	-0.05	4.33	0.81
	WCH	-0.73	0.03	-0.06	-0.06	1.47	0.09
	CCS	1.24	-0.51	-0.17	-0.17	-2.44	0.46
CWD	SCA	-1.05	0.90	0.26	0.26	2.10	0.73
	BYP	-0.64	0.65	-0.55	-0.55	1.60	0.29
	NP	-1.55	-0.04	-0.17	-0.17	3.31	0.30
	WCH	0.54	-0.41	-0.47	-0.47	-0.86	0.41
	CCS	0.95	0.10	-0.91	-0.91	-1.63	0.69
R95p	SCA	-1.56	-0.02	-0.03	-0.03	3.36	0.32
	BYP	-1.67	0.52	-0.19	-0.19	3.45	0.50
	NP	1.33	-0.63	-0.16	-0.16	-2.55	0.64
	WCH	0.21	0.53	-0.63	-0.63	-0.41	0.21
	CCS	-1.07	0.47	-0.49	-0.49	2.37	0.24
R99p	SCA	0.50	-0.75	-0.57	-0.57	-0.78	0.71

	BYP	-0.43	0.78	0.20	0.20	0.63	0.49
	NP	-0.71	0.01	0.28	0.28	1.24	0.25
	WCH	-1.18	0.20	0.00	0.00	2.54	0.22
	CCS	-0.99	0.67	-0.31	-0.31	2.16	0.29
PRCPTOT	SCA	1.21	0.45	0.53	0.53	-2.69	0.43
	BYP	-1.07	0.24	0.43	0.43	2.06	0.40
	NP	-0.79	0.86	-0.11	-0.11	1.67	0.40
	WCH	-1.07	0.68	-0.53	-0.53	2.38	0.32
	CCS	-0.51	0.43	0.05	0.05	0.82	0.29
TXx	SCA	-0.52	-0.30	-0.95	-0.95	1.34	0.62
	BYP	-0.82	0.05	0.51	0.51	1.40	0.42
	NP	-0.72	-0.73	-0.57	-0.57	1.68	0.58
	WCH	0.14	0.00	-0.22	-0.22	-0.19	0.04
	CCS	-0.52	-0.25	0.09	0.09	1.03	0.06
TNx	SCA	-0.46	-0.12	0.52	0.52	0.77	0.19
	BYP	-1.32	-0.33	0.05	0.05	2.66	0.29
	NP	-0.59	-0.66	-0.68	-0.68	1.42	0.62
	WCH	0.18	-0.23	-0.85	-0.85	-0.16	0.53
	CCS	-0.16	-0.21	-0.22	-0.22	0.45	0.07
TXn	SCA	0.69	-0.18	-0.16	-0.16	-1.33	0.13
	BYP	-0.96	-0.28	0.03	0.03	1.95	0.16
	NP	-0.15	0.02	0.02	0.02	0.26	0.01

	WCH	0.11	-0.10	-0.74	-0.74	-0.07	0.34
	CCS	1.16	-0.03	-0.53	-0.53	-2.19	0.44
TNn	SCA	-0.56	-0.17	-0.94	-0.94	1.40	0.54
	BYP	-0.14	-0.52	-0.26	-0.26	0.42	0.21
	NP	0.20	-0.62	-0.59	-0.59	-0.17	0.55
	WCH	-0.23	-0.12	0.61	0.61	0.23	0.22
	CCS	0.96	-0.01	-0.49	-0.49	-1.78	0.36
TN10p	SCA	-0.54	-0.10	-0.89	-0.89	1.33	0.46
	BYP	-0.44	-0.49	-0.28	-0.28	1.04	0.21
	NP	-0.64	-0.38	-0.76	-0.76	1.52	0.50
	WCH	-0.09	0.12	-0.72	-0.72	0.41	0.24
	CCS	-0.16	0.50	-0.36	-0.36	0.40	0.09
TN90p	SCA	-0.57	-0.23	-1.06	-1.06	1.48	0.70
	BYP	-0.27	0.11	-0.11	-0.11	0.41	0.11
	NP	-0.68	-0.21	-0.78	-0.78	1.63	0.42
	WCH	-0.21	-0.04	-0.67	-0.67	0.58	0.25
	CCS	1.38	0.59	-0.41	-0.41	-2.75	0.40
TX10p	SCA	-1.39	0.06	-0.44	-0.44	3.07	0.29
	BYP	0.16	-0.68	-0.25	-0.25	-0.10	0.37
	NP	-0.77	-0.64	-0.69	-0.69	1.82	0.62
	WCH	-0.25	-0.06	-0.41	-0.41	0.50	0.15
	CCS	0.17	-0.24	-0.13	-0.13	-0.28	0.06

TX90p	SCA	-0.56	0.36	-0.66	-0.66	1.44	0.23
	BYP	-0.64	-0.44	0.06	0.06	1.28	0.12
	NP	-0.96	-0.11	-0.82	-0.82	2.22	0.44
	WCH	-0.19	-0.25	-0.83	-0.83	0.58	0.48
	CCS	-0.25	-0.45	0.05	0.05	0.46	0.10
WSDI	SCA	-0.38	0.31	0.09	0.09	0.63	0.14
	BYP	-0.85	-0.20	0.14	0.14	1.61	0.19
	NP	-1.04	-0.12	-0.76	-0.76	2.32	0.42
	WCH	-0.54	-0.07	-0.68	-0.68	1.29	0.27
	CCS	0.61	-0.19	-0.41	-0.41	-1.11	0.24
CSDI	SCA	-0.54	-0.01	-0.18	-0.18	1.12	0.05
	BYP	-0.54	-0.59	-0.10	-0.10	1.17	0.19
	NP	-0.50	-0.30	-0.75	-0.75	1.24	0.43
	WCH	-0.78	0.01	-0.87	-0.87	1.87	0.41
	CCS	-0.90	0.09	-0.11	-0.11	1.82	0.14
DTR	SCA	0.00	0.11	-0.44	-0.44	-0.01	0.12
	BYP	-0.63	-0.34	0.14	0.14	1.17	0.15
	NP	-0.26	-0.28	-1.04	-1.04	0.88	0.73
	WCH	-0.38	-0.59	-0.65	-0.65	0.90	0.55
	CCS	-0.66	0.20	-0.42	-0.42	1.28	0.24
P	SCA	-0.05	0.04	-0.07	-0.07	-0.08	0.12
	BYP	-0.19	0.17	0.35	0.35	0.37	0.14

	NP	0.43	-0.14	0.15	0.15	-0.88	0.04
	WCH	-0.09	-0.11	0.17	0.17	0.06	0.04
	CCS	0.95	-0.22	0.08	0.08	-1.93	0.16
T	SCA	-1.21	0.75	0.38	0.38	2.34	0.76
	BYP	-1.39	0.56	0.20	0.20	2.75	0.57
	NP	-1.79	0.70	-0.01	-0.01	3.65	0.72
	WCH	-1.41	0.43	0.38	0.38	2.79	0.60
	CCS	-1.82	0.44	0.32	0.32	3.59	0.80
PET	SCA	-1.30	0.74	0.36	0.36	2.55	0.77
	BYP	-1.61	0.56	0.07	0.07	3.26	0.60
	NP	-1.86	0.69	-0.12	-0.12	3.85	0.69
	WCH	-1.51	0.48	0.18	0.18	3.07	0.53
	CCS	-1.95	0.44	0.21	0.21	3.91	0.79
ϕ	SCA	0.48	-0.32	-0.24	-0.24	-1.11	0.26
	BYP	0.27	0.00	0.34	0.34	-0.58	0.08
	NP	0.92	-0.27	0.24	0.24	-1.96	0.14
	WCH	0.34	-0.21	0.10	0.10	-0.82	0.06
	CCS	1.48	-0.34	-0.04	-0.04	-2.98	0.43
PDJF	SCA	-0.24	0.06	0.15	0.15	0.17	0.04
	BYP	0.39	0.10	-0.13	-0.13	-0.48	0.08
	NP	0.41	0.24	0.15	0.15	-1.05	0.11
	WCH	0.18	0.00	0.07	0.07	-0.49	0.01

	CCS	0.27	0.21	0.29	0.29	-1.05	0.08
PMAM	SCA	1.51	0.18	-0.18	-0.18	1.98	0.11
	BYP	-1.99	0.34	-0.16	-0.16	2.12	0.27
	NP	1.00	0.64	0.15	0.15	0.15	0.14
	WCH	-0.40	0.45	0.07	0.07	0.97	0.14
	CCS	1.76	0.56	0.07	0.07	0.01	0.07
PJJA	SCA	0.29	0.30	-0.17	-0.17	-1.21	0.16
	BYP	-0.89	0.03	0.13	0.13	-0.25	0.04
	NP	-0.57	-0.01	0.00	0.00	-1.96	0.13
	WCH	-0.44	-0.12	0.00	0.00	-0.91	0.09
	CCS	0.05	-0.08	-0.07	-0.07	-2.75	0.29
PSON	SCA	0.96	-0.32	0.16	0.16	0.49	0.15
	BYP	-0.20	0.10	-0.01	-0.01	0.97	0.04
	NP	0.18	-0.34	0.05	0.05	1.13	0.13
	WCH	0.78	-0.38	0.29	0.29	0.85	0.14
	CCS	0.36	-0.33	-0.02	-0.02	0.41	0.13

Section 5. Detection and attribution analysis for selected clusters in Central America.

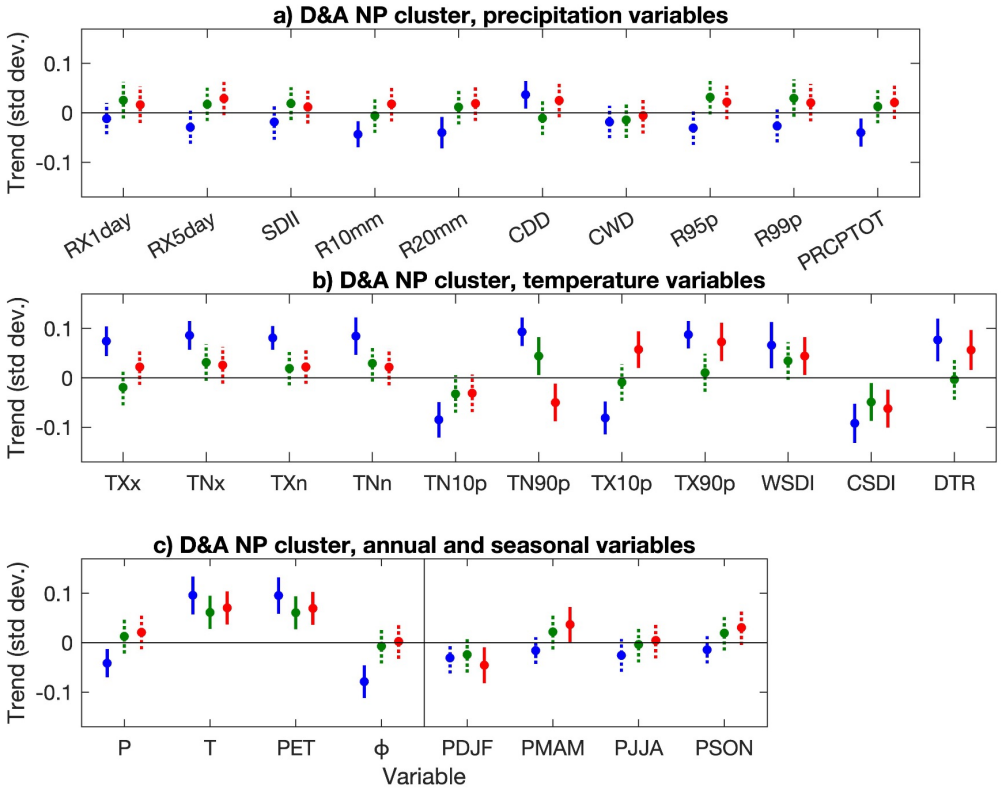

Fig S5 Results of detection and attribution analysis for the North Pacific cluster (NP; see Fig. 1). The analysis was performed for precipitation (top panel) and temperature (middle panel) CLIMDEX extreme indices (definitions in tables S2 and S3 in the Supplementary Information). Also shown in the bottom panel are the analysis for the annual averages of precipitation (P), 2-m temperature (T), potential evapotranspiration (PET) and the ϕ aridity index (defined as P/PET). The four rightmost variables in the bottom panel display the trends of the boreal seasonal precipitation averages. Blue dots represent trends in each standardized variables from a historical run involving an ensemble of 10 models, while the blue confidence intervals are constructed based on the ensemble noise derived from the respective preindustrial control runs. Green dots represent trends based on W5E5 data, with their confidence intervals computed using the synthetic generation described by McKinnon and Deser (2021). Red dots represent trends from the CHIRPs and CHIRTs "observations" (Funk et al. 2015), with the noise levels matching the green methodology. Trends that can (cannot) be detected from the natural variability noise are shown with solid (dotted lines), according to the different methods applied. The trends correspond to the period 1983-2016 for the blue and red analysis, and from 1979 to 2019 for the green analysis

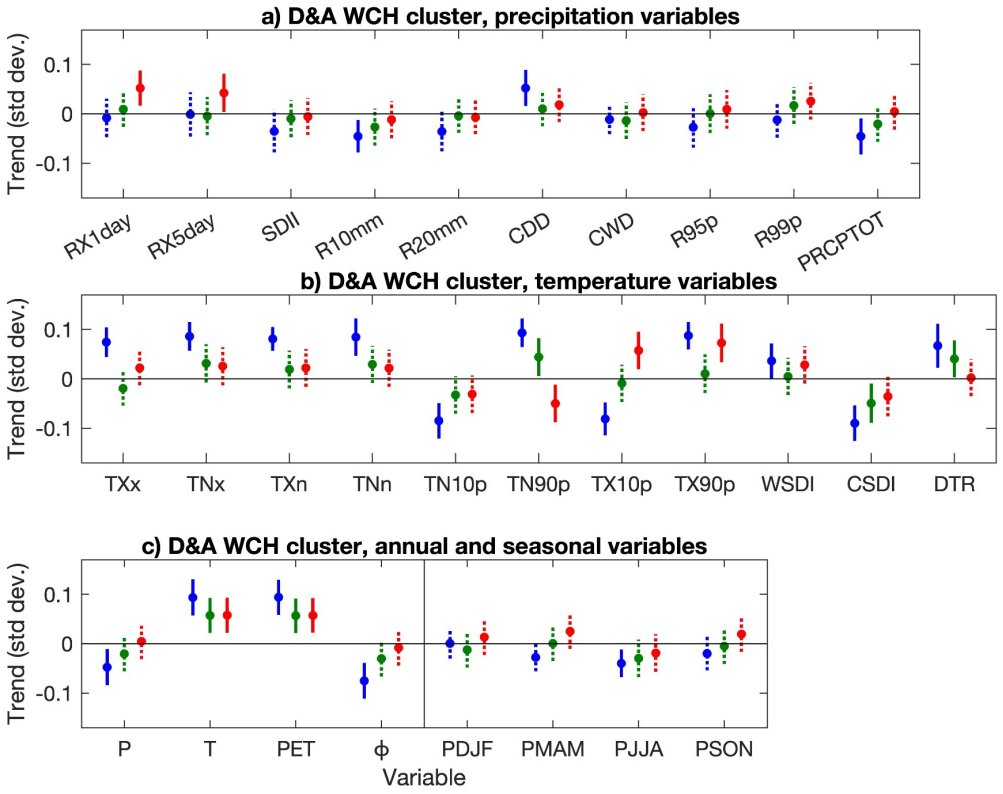

Fig. S6 Same as in Fig. S5 but for the WCH cluster.

Errata

First sentence in the abstract should be read it as:

“We present an analysis to determine whether historical trends in extreme precipitation and temperature indices, as well as in yearly averages of several climate variables, for the Central American region, indicate a sufficient climate signal associated with anthropogenic climate change and, therefore, to assess whether these trends can be explained solely by natural causes.”

On page 15, there is a “) “ missing after in Pascale et al. (2019 .